



**HAL**  
open science

## Isotopic evidence for multiple recycled sulfur reservoirs in the Mangaia mantle plume

J W Dottin, Jabrane Labidi, M G Jackson, J Woodhead, J Farquhar

### ► To cite this version:

J W Dottin, Jabrane Labidi, M G Jackson, J Woodhead, J Farquhar. Isotopic evidence for multiple recycled sulfur reservoirs in the Mangaia mantle plume. *Geochemistry, Geophysics, Geosystems*, 2020. insu-03584471v1

**HAL Id: insu-03584471**

**<https://hal.science/insu-03584471v1>**

Submitted on 5 Oct 2021 (v1), last revised 22 Feb 2022 (v2)

**HAL** is a multi-disciplinary open access archive for the deposit and dissemination of scientific research documents, whether they are published or not. The documents may come from teaching and research institutions in France or abroad, or from public or private research centers.

L'archive ouverte pluridisciplinaire **HAL**, est destinée au dépôt et à la diffusion de documents scientifiques de niveau recherche, publiés ou non, émanant des établissements d'enseignement et de recherche français ou étrangers, des laboratoires publics ou privés.

1  
2  
3  
4  
5  
6  
7  
8  
9  
10  
11  
12  
13  
14  
15  
16  
17  
18  
19

## Isotopic evidence for multiple recycled sulfur reservoirs in the Mangaia mantle plume

J.W. Dottin III<sup>1</sup>, J. Labidi<sup>3</sup>, M.G. Jackson<sup>4</sup>, J. Woodhead<sup>5</sup>, J. Farquhar<sup>1,2</sup>

<sup>1</sup>Department of Geology, University of Maryland, College Park, MD 20742, United States

<sup>2</sup>Earth System Science Interdisciplinary Center, College Park, MD 201742, United States

<sup>3</sup>Université de Paris, Institut de physique du globe de Paris, CNRS, F-75005 Paris, France

<sup>4</sup>Department of Earth Science, University of California, Santa Barbara, CA 93106, United States

<sup>5</sup>School of Earth Sciences, University of Melbourne, Victoria 3010, Australia

Corresponding author: James Wosley Dottin III (jdottin@umd.edu)

### Key Points:

- We report bulk S-isotope compositions of sulfide in melt inclusions of olivines and pyroxenes from Mangaia.
- Isotopic disequilibrium in a single sample record a process of trapping various compositions during magma mixing.
- Data collected identify a new, potentially young, recycled component with negative  $\delta^{34}\text{S}$  and slightly positive  $\Delta^{33}\text{S}$  in HIMU source.

## 20 Abstract

21 Mangaia, an ocean island in the Cook-Austral volcanic chain, is the type locality for the HIMU  
 22 mantle reservoir, and has also been shown to exhibit evidence for recycled sulfur with  
 23 anomalous  $\delta^{34}\text{S}$  and  $\Delta^{33}\text{S}$  that has been attributed an Archean origin. Here we report bulk S  
 24 isotope data from sulfide inclusions in olivine and pyroxene phenocrysts from one of the  
 25 previously analyzed and four additional Mangaia basalts to further test for the prevalence of  
 26 anomalous S in the HIMU mantle source feeding Mangaia. We document compositions that  
 27 range from  $-5.13\text{‰}$  to  $+0.21\text{‰}$  ( $\pm 0.3$   $2\sigma$ ),  $+0.006\text{‰}$  to  $+0.049\text{‰}$  ( $\pm 0.016$   $2\sigma$ ),  $-0.81\text{‰}$  to  $+0.69\text{‰}$   
 28 ( $\pm 0.3$   $2\sigma$ ) for  $\delta^{34}\text{S}$ ,  $\Delta^{33}\text{S}$ , and  $\Delta^{36}\text{S}$  respectively. These data extend the range of measured  
 29 compositions and suggest S-isotope heterogeneity in the HIMU mantle source at Mangaia. We  
 30 show that S-isotope compositions of bulk sulfide in olivine is not in isotopic equilibrium with  
 31 bulk sulfide in pyroxene from the same samples and that samples from a confined area (M4,  
 32 M10, M12, & M13) in the northern central part of the island show a distinct covariation for  $\delta^{34}\text{S}$   
 33 and  $\Delta^{33}\text{S}$ . This isotopic variation (forming an array) suggests mixing of sulfur from two sources  
 34 that were captured at different stages of crystallization by phenocrysts in the Mangaia HIMU  
 35 sulfur endmember.

## 36 Plain Language Summary

37 The sulfur isotope composition of the mantle is heterogenous from crust formation and recycling  
 38 continental and oceanic crust. Basalts, from an intraplate volcanic hotspot volcano in the Pacific  
 39 ocean, Mangaia, show isotopic evidence for hosting Archean related sulfur that is sourced from a  
 40 recycled oceanic crustal component. The prevalence of this Archean related sulfur in the plume  
 41 source that feeds Mangaia is not well constrained. In this work, we present sulfur isotope data on  
 42 sulfur from minerals that crystallized deep in the magma chamber and identify a new, potentially  
 43 younger, recycled sulfur source that demonstrates the diversity of materials mixing in the magma  
 44 chamber prior to eruption.

## 45 1 Introduction

46 Covariations in the radiogenic isotope signature of strontium, neodymium and lead seen  
 47 in various Mid-Ocean Ridge Basalts (MORB) and Ocean Island Basalts (OIB) have been used to  
 48 identify distinct compositional reservoirs that exist in the mantle as a result of melt removal and  
 49 recycling of oceanic and continental crust. These reservoirs have been termed Depleted MORB  
 50 Mantle (DMM), Enriched Mantle I and II (EM I, EM II), and HIMU (high  $\mu=^{238}\text{U}/^{204}\text{Pb}$ ).  
 51 Depleted MORB mantle is characterized as having relatively low  $^{206,207,208}\text{Pb}/^{204}\text{Pb}$  and  $^{87}\text{Sr}/^{86}\text{Sr}$   
 52 but high  $^{143}\text{Nd}/^{144}\text{Nd}$ , and argued to have formed from the process of melt removal during crust  
 53 formation (Salters and Stracke, 2004; Workman and Hart, 2005). HIMU is characterized by high  
 54  $^{206,208}\text{Pb}/^{204}\text{Pb}$  (and variable  $^{207}\text{Pb}/^{204}\text{Pb}$ ), low  $^{87}\text{Sr}/^{86}\text{Sr}$ , and intermediate  $^{143}\text{Nd}/^{144}\text{Nd}$ . The HIMU

55 reservoir is thought to have formed from the recycling of oceanic crust that experienced Pb loss  
56 from sulfides during subduction followed by the ingrowth of radiogenic Pb due to a high  
57  $^{238}\text{U}/^{204}\text{Pb}$  ('high  $\mu$ ') time integrated ratio (e.g Chauvel et al., 1992; Kelley et al., 2005) with a  
58 wide range of proposed formation ages of 550 Ma to 3.0 Ga (Hauri and Hart, 1993; Thirlwall,  
59 1997; Nebel et al., 2013; Mazza et al., 2019).

60 Mangaia, located in the Cook-Austral volcanic chain, is the type locality for the HIMU  
61 mantle reservoir that, together with Bermuda, preserve the highest reported radiogenic  
62  $^{206}\text{Pb}/^{204}\text{Pb}$  isotope compositions of any OIB locality suggesting an old, and recycled mantle  
63 source (Hauri and Hart, 1993; Woodhead, 1996; Mazza et al., 2019). Jackson and Dasgupta  
64 (2008) and Cabral et al. (2014) argue that HIMU basalts are associated with a carbonated mafic  
65 source on the basis of major element characteristics (low  $\text{SiO}_2$  and high  $\text{CaO}/\text{Al}_2\text{O}_3$ ) and elevated  
66 volatile contents of  $\text{CO}_2$ . Weiss et al. (2016) suggest the HIMU mantle source of Mangaia was  
67 metasomatized by carbonatitic fluids and imply a connection to recycling processes. The sulfur  
68 isotope composition of sulfides in sulfide inclusions trapped in magmatic olivine from Mangaia  
69 basalts has been measured in-situ using secondary ion mass spectrometry (SIMS) and also using  
70 conventional bulk isotope methods (Cabral et al. 2013). The  $\delta^{34}\text{S}$  values reported from Mangaia  
71 ( $\sim -17\text{‰}$  to  $-3\text{‰}$ ) are depleted in heavy isotopes compared to bulk sulfur isotope measurements of  
72 MORB (Mid Ocean Ridge Basalt) glasses (average  $\delta^{34}\text{S}$  of Pacific-Antarctic basalts =  
73  $-0.89 \pm 0.11$  ( $1\sigma$ ), Labidi et al., 2014) and additionally show small but significant negative  $\Delta^{33}\text{S}$   
74 in two samples by SIMS, down to  $-0.24 \pm 0.15\text{‰}$  ( $2\sigma$ ) (weighted average =  $-0.25 \pm 0.07\text{‰}$ ,  $2\sigma$ ) and  
75  $-0.35 \pm 0.23\text{‰}$  (weighted average =  $-0.34 \pm 0.08\text{‰}$ ) in MGA-B-25 and MGA-B-47, respectively.  
76 Taken together, the data collected via SIMS and conventional bulk S isotope measurements  
77 reveal compositions that are consistent with a subducted component in the source of Mangaia

78 melts that hosts Archean sulfur that experienced mass independent fractionation (Cabral et al.,  
79 2013). What remains unanswered is whether anomalous Archean S is common in the HIMU  
80 mantle reservoir sampled by Mangaia, or whether other Mangaia basalts contain what might be  
81 considered more typical mass-dependent sulfur.

82 Here, we present bulk S-isotope compositions ( $\delta^{34}\text{S}$ ,  $\Delta^{33}\text{S}$  and  $\Delta^{36}\text{S}$ ) of sulfide inclusions  
83 within magmatic olivine and clinopyroxene phenocrysts from five Mangaia samples. These  
84 olivine and clinopyroxene phenocrysts trap sulfide inclusions during their growth at depth in the  
85 magma chamber and, like melt inclusions (e.g. Sobolev and Shimizu, 1993), they may shed light  
86 on melt mixing of diverse sources. Our data provide new constraints on the various recycled  
87 components that dominates HIMU mantle melts feeding lavas at Mangaia.

## 88 **2 Samples and Methods**

89

90 We present new multiple sulfur isotope data on 5 basaltic samples from Mangaia: MGA-B-  
91 25, M4, M10, M12, and M13. Samples are from a road cut along the northeast side of the island  
92 (MGA-B-25) and from Vau Roa stream Valley (M4, M10, M12, and M13). Samples previously  
93 analyzed (Cabral et al., 2013) using SIMS and discussed in this manuscript are from a road cut  
94 adjacent to a stream north of Tamarua village on the south side of the island (MGA-B-47) and a  
95 small outcrop revealed by a road cut near a stream on the south side of the island (MG1001B).  
96 The work by Cabral et al. (2013) also presents a bulk sulfide measurement from an olivine  
97 separate of MGA-B-47. Further, note that MGA-B-25 was analyzed in Cabral et al. (2013) but  
98 only using SIMS methods. We analyzed newly prepared aliquots of minerals from MGA-B-25,  
99 while M4, M10, M12, and M13 (n=4) are samples that have not previously been analyzed for  
100 sulfur isotopes. With these new measurements we are able to (1) test for S-isotope heterogeneity

101 at different locations on the island (possibly related to separate flows) and (2) evaluate the  
102 prevalence of negative  $\Delta^{33}\text{S}$  in MGA-B-25 and Mangaia basalts generally.

103

## 104 2.1 Acid digestion

105

106 All samples are olivine and clinopyroxene phenocryst separates that were hand-picked and  
107 cleaned by sonication in preparation for S isotope analyses. Crushed and weighed Ol and Px  
108 mineral separates were placed into Teflon reaction vessels for hydrofluoric acid digestion using  
109 methods developed by Labidi et al. (2012) for the liberation of sulfide from silicates. Note these  
110 methods have demonstrated the ability to digest and consistently receive  $100\% \pm 5\%$  of S as  
111 sulfide powders as well as sulfides dissolved in silicate melts (Labidi et al., 2012). Sulfides were  
112 extracted in this study, as the method used here only extracts sulfur of reduced valence, leaving  
113 behind sulfate if present in the samples. The digestion apparatus was first purged for  $\sim 15$   
114 minutes with  $\text{N}_2$ . After purging, the samples were acidified and digested in a heated solution (70-  
115  $80^\circ\text{C}$ ) of 3.2M  $\text{CrCl}_2$ , 12M  $\text{HCl}$ , and 29M  $\text{HF}$  in the amounts of 10 ml, 5 ml, and 5ml  
116 respectively. During this digestion, sulfide was released as  $\text{H}_2\text{S}$ , bubbled ( $\sim 3$ -5 bubbles every  $\sim 1$ -  
117 2 seconds) through a water trap to remove acid vapors, before being bubbled and trapped in  
118 weakly acidic  $\text{AgNO}_3$  where S is precipitated as  $\text{Ag}_2\text{S}$ . The  $\text{Ag}_2\text{S}$  was centrifuged and rinsed 3  
119 times with Milli-Q water. After rinsing, the  $\text{Ag}_2\text{S}$  was dried at  $\sim 70^\circ\text{C}$  and subsequently weighed  
120 to determine sulfur concentration.

## 121 2.2 Fluorination

122  
 123 The weighed  $\text{Ag}_2\text{S}$  was wrapped in foil and placed into nickel reaction tubes 3-5 times  
 124 excess  $\text{F}_2$ . Reactions between  $\text{Ag}_2\text{S}$  and  $\text{F}_2$  occurred at  $\sim 250^\circ\text{C}$  for at least 12 hours. The product  
 125  $\text{SF}_6$  was separated from residual  $\text{F}_2$  by freezing into a liquid-nitrogen-cooled trap. Residual  $\text{F}_2$   
 126 was passivated through a reaction with heated ( $\sim 110^\circ\text{C}$ )  $\text{KBr}$  salt. After all fluorine was  
 127 passivated, the liquid nitrogen trap was replaced by an ethanol slush ( $\sim -108^\circ\text{C}$  to  $-115^\circ\text{C}$ ) to  
 128 retain co-condensed  $\text{HF}$  and the  $\text{SF}_6$  was sublimated into a separate liquid-nitrogen-cooled trap,  
 129 from which it was injected into a gas chromatograph (GC) with a 1/8-inch diameter, 6-foot long  
 130 Haysep-Q<sup>TM</sup> GC column and a 5A GC column using a helium flow rate of 20 mL/min.  $\text{SF}_6$  was  
 131 monitored while passing through the GC and captured in liquid nitrogen cooled metal coils.  
 132 Once captured, the  $\text{SF}_6$  was thawed to determine procedural yields as pressure and lastly, stored  
 133 in individual glass manifolds.

## 134 2.3 Mass spectrometry

135  
 136 Isotopic variations of the four stable isotopes of sulfur ( $^{32}\text{S}$  (95.2%),  $^{33}\text{S}$  (0.75%),  $^{34}\text{S}$   
 137 (4.25%), and  $^{36}\text{S}$  (0.02%)) were determined using gas source mass spectrometry of purified  $\text{SF}_6$ .  
 138 Measurements were made by monitoring  $\text{SF}_5^+$  ion beams at  $m/z$  of 127, 128, 129, and 131 of the  
 139 purified  $\text{SF}_6$ . Each Sample underwent three measurements that consists of eight 26-second cycles  
 140 measuring the sample and the reference gas. Data are reported in per mil using the following  
 141 notation:

$$142 \quad \delta^{33}\text{S} = [((^{33}\text{S}/^{32}\text{S})_{\text{sample}} / (^{33}\text{S}/^{32}\text{S})_{\text{CDT}}) - 1]$$

$$143 \quad \delta^{34}\text{S} = [((^{34}\text{S}/^{32}\text{S})_{\text{sample}} / (^{34}\text{S}/^{32}\text{S})_{\text{CDT}}) - 1]$$

$$144 \quad \delta^{36}\text{S} = [((^{36}\text{S}/^{32}\text{S})_{\text{sample}} / (^{36}\text{S}/^{32}\text{S})_{\text{CDT}}) - 1]$$

145

$$146 \quad \Delta^{33}\text{S} = [((^{33}\text{S}/^{32}\text{S})_{\text{sample}} / (^{33}\text{S}/^{32}\text{S})_{\text{CDT}}) - ((^{34}\text{S}/^{32}\text{S})_{\text{sample}} / (^{34}\text{S}/^{32}\text{S})_{\text{CDT}})^{0.515}]$$

$$147 \quad \Delta^{36}\text{S} = [((^{36}\text{S}/^{32}\text{S})_{\text{sample}} / (^{36}\text{S}/^{32}\text{S})_{\text{CDT}}) - ((^{34}\text{S}/^{32}\text{S})_{\text{sample}} / (^{34}\text{S}/^{32}\text{S})_{\text{CDT}})^{1.9}]$$

148 Analyses are normalized to analyses of Canyon Diablo Troilite on a scale that place IAEA-S1 at

149 a composition of  $\delta^{34}\text{S} = -0.401$ ,  $\Delta^{33}\text{S} = 0.116$ ,  $\Delta^{36}\text{S} = -0.796$  (Antonelli et al., 2014). For

150 normalization, raw delta values from sample analysis are converted to ratios and normalized to

151 the isotope ratio associated with measurements of CDT (Antonelli et al. 2014).  $\Delta^{33}\text{S}$  and  $\Delta^{36}\text{S}$  are

152 calculated from the CDT normalized delta values. Uncertainties on measurements are estimated

153 from the long-term reproducibility on measurements (including wet chemistry, fluorination, and

154 mass spectrometry) of standard materials and are 0.3, 0.016, and 0.3 ( $2\sigma$ ) for  $\delta^{34}\text{S}$ ,  $\Delta^{33}\text{S}$ , and

155  $\Delta^{36}\text{S}$  respectively. As a test of our methods and uncertainty, we have analyzed MORB glasses

156 that were previously analyzed in (Labidi et al., 2014), namely, PAC2 DR 32-1G, PAC2 DR 06-

157 6G, and PAC1 CU 03-3G and one MORB glass that is not reported, PAC2 DR 20-04 (see

158 supplementary Table 1). When a small difference in the calibration between the two labs (CDT

159 here versus a V-CDT calibration described in Labidi et al., 2014) are taken into account, the data

160 are are reproducible and within uncertainty of measurements between both labs. The values of

161 CDT normalized to IAEA S-1 in the two studies are:  $\delta^{34}\text{S} = -0.401 \pm 0.15\%$ ,  $\Delta^{33}\text{S} =$

162  $+0.116 \pm 0.008\%$ , and  $\Delta^{36}\text{S} = -0.796 \pm 0.080\%$  for UMD and  $\delta^{34}\text{S}_{(\text{V-CDT})} = -0.14 \pm 0.52$ ,  $\Delta^{33}\text{S} =$

163  $+0.106 \pm 0.008$ , and  $\Delta^{36}\text{S} = -0.782 \pm 0.140$  for Labidi et al. (2014) (all 2SD).

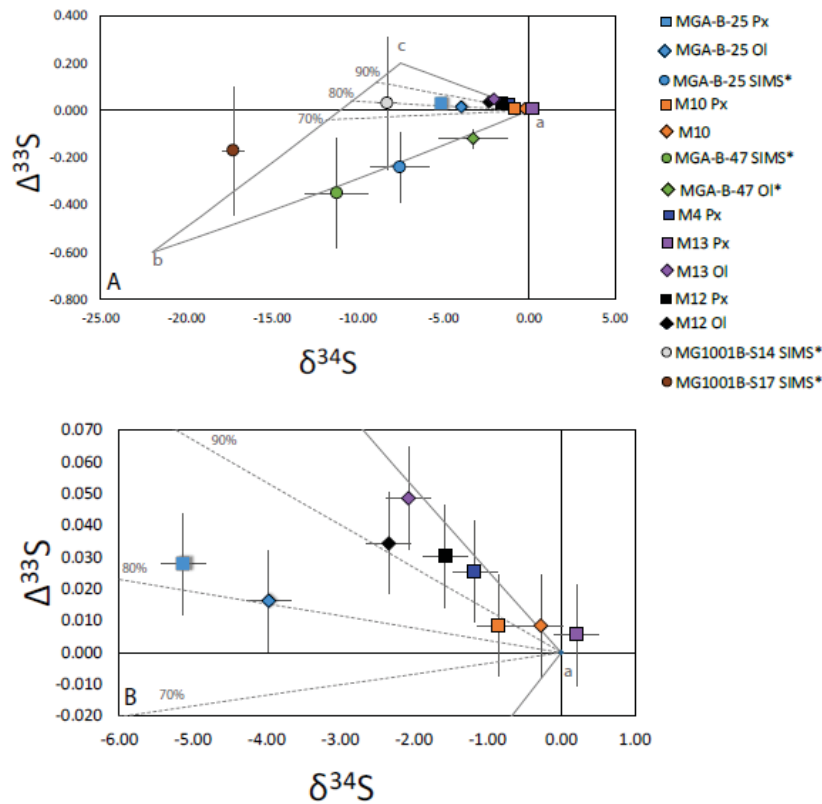
164

165

### 166 **3 Results**

167

168 Bulk sulfur isotope compositions of sulfide minerals hosted in olivine and pyroxene  
 169 mineral separates from Mangaia basalts are reported in Table 1 and illustrated in figure 1 and  
 170 figure 2. We extracted 0.54 mg to 1.57 mg of  $\text{Ag}_2\text{S}$  from  $\sim 300$  to 400 mg of sample resulting in  
 171 sulfur concentrations that range from 96 to 333 ppm. S concentration in Ol and Px from the same  
 172 sample do not match and show no systematic S concentration in olivine versus pyroxene  
 173 separates (Table 1).



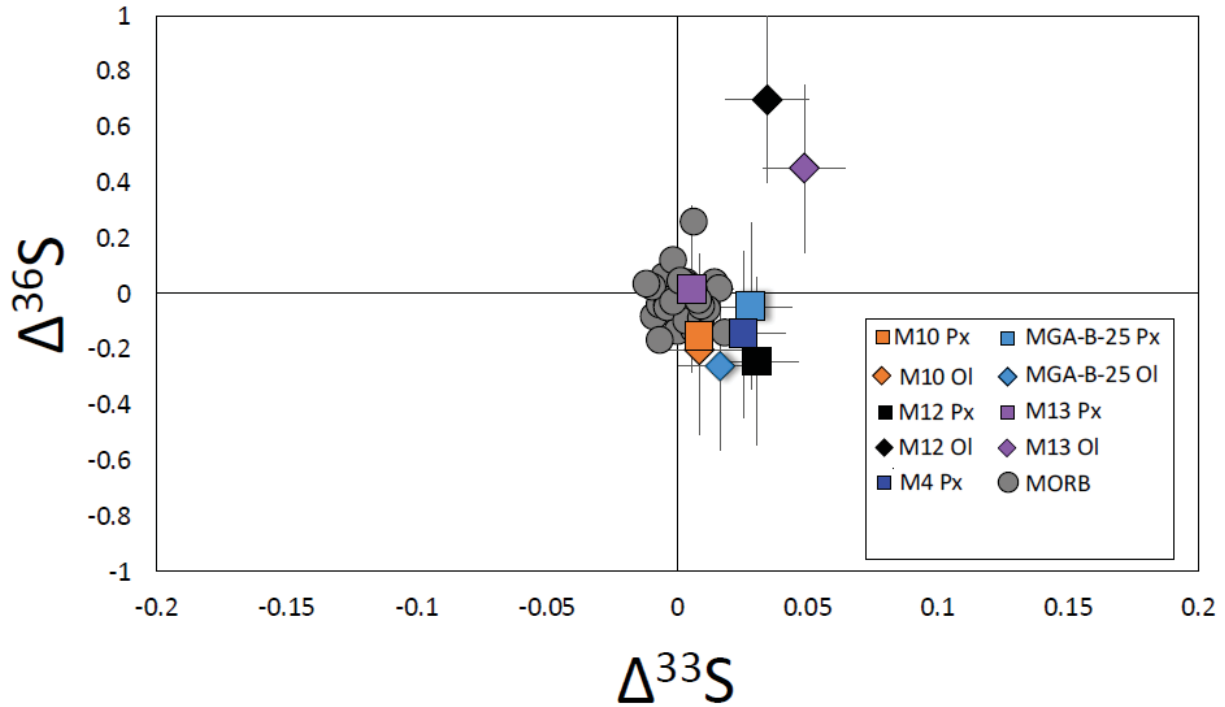
174

175 Figure 1.  $\delta^{34}\text{S}$  vs.  $\Delta^{33}\text{S}$  for bulk sulfide data from sulfide inclusions in olivine and pyroxene  
 176 phenocrysts. We also plot a mixing triangle between (a) the convective mantle [ $\delta^{34}\text{S}= 0$ ,  $\Delta^{33}\text{S}= 0$ ],  
 177 (b) the proposed recycled endmember from Cabral et al. (2013) [ $\delta^{34}\text{S}= -22$ ,  $\Delta^{33}\text{S}= -0.6$ ], and  
 178 (c) our new proposed second recycled endmember [ $\delta^{34}\text{S}= -7.5$ ,  $\Delta^{33}\text{S}= +0.2$ ]. The dashed mixing  
 179 lines within the triangle show that the S-isotope composition of bulk sulfide measurements  
 180 represent a mixture of  $\sim 80\%$  the recycled (c) component, providing a potential explanation for  
 181 the mismatch between the SIMS analysis and the bulk measurement.

182

183 The  $\delta^{34}\text{S}$  compositions measured range from -5.1‰ to +0.2‰ ( $\pm 0.3\ 2\sigma$ ). Sulfide minerals  
184 hosted in olivine are not in isotopic equilibrium with sulfide minerals from pyroxene in the same  
185 sample showing -4.0‰ and -5.1‰ for MGA-B-25 Ol and MGA-B-25 Px respectively, -0.3‰  
186 and -0.9‰ for M10 Ol and M10 Px respectively, -2.3‰ and -1.6‰ for M12 Ol and M12 Px  
187 respectively and -2.1‰ and 0.2‰ M13 Ol and M13 Px respectively (figure S3). This reflects  
188 remarkable intrasample (olivine versus pyroxene in the same lava) and intersample (olivines and  
189 pyroxenes from different samples)  $\delta^{34}\text{S}$  variability in Mangaia lavas. However, there is no  
190 relationship between the magnitude of the  $\delta^{34}\text{S}$  value and type of mineral separate. There is also  
191 no systematic fractionation among the mineral separates from the same sample.

192 The  $\Delta^{33}\text{S}$  and  $\Delta^{36}\text{S}$  range from +0.002‰ to +0.049‰ and -0.81‰ to +0.69‰,  
193 respectively.  $\Delta^{33}\text{S}$  values of sulfide in Ol and Px from the samples measured are similar with  
194 exception of one sample (M13) showing  $\Delta^{33}\text{S} = +0.049‰$  and +0.006‰ for Ol and Px,  
195 respectively. Similarly,  $\Delta^{36}\text{S}$  values are similar for sulfides in pyroxene and olivine, with the  
196 exception of M12 showing  $\Delta^{36}\text{S} = +0.7‰$  and -0.3‰ for Ol and Px, respectively. A subset of  
197 samples (M4, M10, M12, and M13) yield a rough negative correlation between  $\delta^{34}\text{S}$  and  $\Delta^{33}\text{S}$   
198 (Fig. 3). With the exception of two data points (M13 Ol, and M12 Ol), the data plot at slightly  
199 higher  $\Delta^{33}\text{S}$  and lower  $\Delta^{36}\text{S}$  compared to previously published data from MORB (figure 2).



200

201 Figure 2.  $\Delta^{33}\text{S}$  vs.  $\Delta^{36}\text{S}$  for bulk sulfide data from sulfide inclusions in olivine and pyroxene  
 202 phenocrysts. With the exception of two data points from sulfide in olivine (M12 OI and M13 OI),  
 203 the data overlap with data from MORB (Labidi et al., 2013; Labidi et al., 2014; Labidi and  
 204 Cartigny, 2016)

205

206

#### 207 4. Discussion

208

209 An unusual observation of HIMU mantle sampled at Mangaia made by Cabral et al.  
 210 (2013), is the negative  $\delta^{34}\text{S}$  and the presence of S-MIF observed in individual sulfides by SIMS  
 211 and by  $\text{SF}_6$  techniques similar to those used here. The signatures observed by Cabral et al.  
 212 (2013) yielded a field extending from  $\delta^{34}\text{S}$  of  $-3.3 (\pm 2\text{‰})$  to  $-17.3 \text{‰} (\pm 0.6\text{‰})$  and with near-zero  
 213 to negative  $\Delta^{33}\text{S}$ . The observation of samples with negative  $\Delta^{33}\text{S}$  that were measured both by  
 214 SIMS and with one measurement by  $\text{SF}_6$  ( $-0.12 \pm 0.04\text{‰}$ ,  $2\sigma$ ) carried out at UMD (on sample

215 MGA-B-47) is ascribed to the presence of subducted and recycled Archean components in the  
216 Mangaia source.

217         The data collected in this study on sulfide inclusions in mineral separates of Ol and Px  
218 from Mangaia also shows a range of  $\delta^{34}\text{S}$ , but do not extend to values as negative as those  
219 presented in Cabral et al. (2013) (-5.2‰ to +0.2‰). Our data also lack the negative  $\Delta^{33}\text{S}$  values  
220 seen in Cabral et al. (2013) and extend from to +0.006 to +0.049‰ ( $\pm 0.016$ ‰). Our data include  
221 analyses of sulfur from phenocrysts of one sample studied by Cabral et al. (2013) [MGA-B-25]  
222 for which they report a negative  $\Delta^{33}\text{S}$  by SIMS, because this sample had not been analyzed using  
223 the  $\text{SF}_6$  method by Cabral et al. (2013). Cabral et al. (2013) reported a  $^{33}\text{S}$  depletion (-  
224  $0.12 \pm 0.04$ ‰,  $2\sigma$ ) in an olivine separate from MGA-B-47. This was based on a measurement in  
225 our laboratory using the same fluorination and mass spectrometry as that is described in the  
226 methods section of this manuscript, but with a wet chemistry protocol involving hydrochloric  
227 acid and Cr(II) to digest sulfide minerals. MGA-B-47 was not reanalyzed here due to lack of  
228 available olivine material with inclusions. The protocol we use here includes HF, in addition to  
229 HCl and Cr(II), after Labidi et al. (2012). The HF techniques are more efficacious at digesting  
230 silicate and thus can extract sulfides trapped within phenocrysts which may be missed by the  
231 HCl + Cr(II) protocol used in Cabral et al. (2013). While the sulfide concentrations we observe  
232 (96 to 333 ppm) are higher than those reported in Cabral et al. (2013) for the  $\text{SF}_6$  analysis of  
233 olivine from MGA-B-47 (~30 ppm), we cannot say whether this is due to some sulfide loss  
234 during sample processing in the laboratory, or whether this reflects a lower sulfide content for  
235 the material from MGA-B-47 compared to the samples studied here. Regardless, both datasets  
236 (from Cabral et al. (2013) and this study) reveal significant variability for both  $\delta^{34}\text{S}$  and  $\Delta^{33}\text{S}$  that  
237 reflect some aspect of the history of these materials. We discuss below the arguments that

238 support an origin associated with mixing of sulfur from different sources at the time of  
239 phenocryst formation.

#### 240 4.1 Phenocrysts and links to sulfide concentration

241  
242 A unique aspect of this work is that our samples are not whole rock samples or glasses,  
243 but rather phenocryst separates containing sulfide inclusions (Cabral et al., 2013). Sulfur is  
244 incompatible and thus not incorporated in olivine and pyroxenes structures (Peach et al., 1990;  
245 Gaetani and Grove, 1997). Digestion of sulfide from inclusions such as those documented by  
246 Cabral et al. (2013, 2014) is also the most straightforward way to explain the amount of sulfur  
247 we see from digestion of phenocrysts. We observe between 100 and 300 ppm S in the bulk  
248 mineral separates (Table 1). Considering a silicate melt inclusion from Mangaia typically hosts  
249 ~1000-2000 ppm S (Cabral et al., 2014), olivines would be required to be composed of 5-20 wt%  
250 melt inclusions to account for our concentration data. This is significantly more than the < 0.1  
251 vol% observed for phenocrysts (Cabral et al., 2014). Our S concentrations, however, are  
252 consistent with the presence of exsolved sulfide inclusions, which consist of approximately 32  
253 wt% S, and thus require <0.02 vol% as sulfide inclusions in phenocrysts.

254 Trapping of sulfide liquids by growing phenocrysts is supported by observations in  
255 previous work: near-perfect spherical-shaped sulfide inclusions were observed in olivine (often  
256 coexisting with silicate melt inclusions) by Cabral et al. (2013, 2014). The sulfide droplets were  
257 shown to display an association of Cu, Ni and Fe sulfides that exsolved upon further cooling  
258 (Cabral et al., 2013), which is typical of magmatic sulfides observed in MORBs (Peach et al.,  
259 1990). For sulfide to be trapped as inclusions in phenocrysts, the associated melt must be sulfide  
260 saturated and contain coexisting sulfide liquid droplets. Such liquids could have exsolved from

261 the silicate melt as a result of changes in melt composition associated with phenocryst formation  
262 or other processes. Liquid sulfide droplets would subsequently be trapped by growing olivine  
263 and pyroxene phenocrysts. Note that the amount of sulfide inclusions in any of the phenocrysts  
264 must reflect a variety of factors, including the level of sulfide saturation and the behavior of  
265 sulfide liquids and phenocrysts during the time leading up to and including entrapment. Similar  
266 to melt inclusions not yielding straightforward information for characterizing the liquid/mineral  
267 ratios of parental melts, the amount of sulfide inclusions may not directly constrain the sulfide  
268 concentration of the parent melt(s).

269 Melt inclusions in olivine phenocrysts from Mangaia record pressures of entrapment  
270 between 250 bar to 1.75 kbar that translate into approximately 0.9 to 6.4 km depth (Cabral et al.,  
271 2014) and magmatic melt temperatures of  $>1200^{\circ}\text{C}$ . Again, at these conditions sulfides are above  
272 the liquidus (Craig and Kullerud, 1968). At these pressures, available thermodynamic models  
273 argue against sulfur degassing as a significant, or even likely, process (Gaillard et al., 2011;  
274 Burgisser et al., 2015). Once trapped, the phenocrysts encapsulate and isolate sulfide sulfur from  
275 further processing such as degassing upon eruption and post-eruption weathering, and provide  
276 snapshots of the diversity of magma chamber compositions prior to mixing and eruption. This  
277 process is analogous to the entrapment of melt inclusions which reveal heterogeneities inherited  
278 from mantle sources, before late mixing and eruption (e.g. Sobolev and Shimizu, 1993).

279

#### 280 4.2 Covariation of $\delta^{34}\text{S}$ and $\Delta^{33}\text{S}$ in Mangaia samples M4, M10, M12 and M13

281

282 We observe covariation of  $\delta^{34}\text{S}$  and  $\Delta^{33}\text{S}$  for sulfide from bulk Ol and Px in samples M4,  
283 M10, M12, and M13. It is conceivable that the covariation is the result of a high temperature

284 process that yields mass dependent fractionation. One may suggest that the Mangaia melts  
285 started with near-zero  $\delta^{34}\text{S}$  and  $\Delta^{33}\text{S}$  values, similar to MORB values (Labidi et al., 2014), and  
286 subsequently evolved towards low  $\delta^{34}\text{S}$  and high  $\Delta^{33}\text{S}$ . However, the change of  $\Delta^{33}\text{S}$  with  $\delta^{34}\text{S}$   
287 is not explained by the typical 0.515 exponent for high-temper

288 ature isotopic fractionations (Hulston and Thode, 1965; Cao and Liu, 2011). An exponent  
289 of  $0.499\pm 0.005$  is needed to fit the  $\delta^{33}\text{S} - \delta^{34}\text{S}$  data (figure S2) from this study (specifically that  
290 of M4, M10, M12, and M13). Although observations of exponents outside of 0.515 have been  
291 proposed for lower temperature processes (e.g., Deines, 2003; Eldridge and Farquhar, 2018), we  
292 know of none that translate to the conditions at high temperature.

293 While the armoring of sulfides by phenocrysts likely makes them immune to effects of  
294 degassing, we examine degassing further since it is a common process in basalts and, as such, is  
295 a typical explanation for shifts to negative (or positive)  $\delta^{34}\text{S}$  (Mandeville et al. 2009, De Moor et  
296 al. 2013, Beaudry et al., 2018). Given the mass fractionation scenario proposed by (Fiege et al.,  
297 2015) at QFM (quartz-fayalite-magnetite) redox conditions, a loss of 85% of the sulfur as S(IV)  
298 during equilibrium (i.e., closed system) degassing would be required to achieve a  $\delta^{34}\text{S}$  shift of ~  
299 3 ‰. This is insufficient to account for the range of observed  $\delta^{34}\text{S}$  in our dataset and also that  
300 observed by Cabral et al. (2013). There is also no clear evidence that degassing can explain the  
301 change of  $\Delta^{33}\text{S}$  with  $\delta^{34}\text{S}$  from 0.515 by significant amounts. Although analyses of degassed  
302 OIB show shifts for  $\delta^{34}\text{S}$ , they show no significant  $\Delta^{33}\text{S}$  variations, even when large  $\delta^{34}\text{S}$   
303 fractionations are produced (Beaudry et al., 2018; Dottin III et al., 2020).

304 Partitioning of sulfur to S(VI) (sulfate) is also known to shift the  $\delta^{34}\text{S}$  of residual sulfide  
305 to negative values. A case has been made for the presence of sulfate in OIBs (Jugo et al., 2010;  
306 Labidi et al., 2015). The equilibrium fractionation between sulfide and sulfate for  $\delta^{34}\text{S}$  is ~3‰ at

307 1200°C (Mandeville et al., 2009 and references within). The possibility that this accounts for a  
308  $^{34}\text{S}$  depletion of the magnitude we observe would require a significant partitioning of sulfur to  
309 sulfate, and a sulfate/ $\Sigma$ sulfur ratio greater than values seen in OIB (e.g., 0.2 observed in Samoan  
310 lavas in Labidi et al., 2015). In the extreme case where 50% of total sulfur in the melt is sulfate,  
311 sulfides would be shifted from the bulk sulfur composition by  $\sim 1.5\%$ . This fractionation is not  
312 large enough to account for the  $^{34}\text{S}$  depletion observed in the Mangaia sulfide inclusions.  
313 Furthermore, there is no evidence that, at high temperature, sulfide and sulfate would co-exist  
314 with distinct  $\Delta^{33}\text{S}$  values resulting from fractionation with a mass dependent exponent different  
315 from 0.515.

316 Altogether, we conclude that there is no reasonable process identified to explain the  $\delta^{34}\text{S}$   
317 and  $\Delta^{33}\text{S}$  covariation among sample M4, M10, M12, and M13. We argue that, instead, the  
318 covariation is rather likely caused by mixing processes in the mantle sources prior to eruption.  
319 Most of our data are accounted for by two-component mixing, between the ambient mantle and a  
320 component with low  $\delta^{34}\text{S}$  and positive  $\Delta^{33}\text{S}$  (Figure 1A, endmembers a and c). Olivine and  
321 pyroxene separates from a given sample are in S isotope disequilibrium: they do not record  
322 identical  $\delta^{34}\text{S}$ - $\Delta^{33}\text{S}$  compositions. Instead, the data from the various mineral separates plot along  
323 the two-component mixing array  $\delta^{34}\text{S}$ - $\Delta^{33}\text{S}$  space (figure 1). This indicates a contribution of two  
324 isotopically distinct magma sources that are heterogeneously delivered to the magma mixture  
325 and sampled by various phenocrysts in a given sample. Note that MGA-B-25 (measured via  
326 IRMS) does not fall along the two-component mixing relationship between endmembers a and c.  
327 We suggest this reflects the contribution of a third component: the recycled endmember  
328 identified in Cabral et al (2013). We show in figure 1A that this sample can be accounted for by

329 a mixture between the ambient mantle, the endmember identified in Cabral et al. (2013) (Figure  
330 1, endmember b), and the endmember identified in this study (Figure 1, endmember c).

331 The heterogeneous contributions of these three components recorded in phenocrysts of  
332 our samples is in agreement with previous arguments for magma mixing prior to eruption at  
333 Mangaia. This is supported by (1) highly variable forsterite content of olivine from individual  
334 Mangaia lavas and (2) Pb isotopic variability in individual olivine-hosted melt inclusions in  
335 Mangaia lavas (Saal et al., 1998) (but see Paul et al. (2011) and Cabral et al. (2014), who identify  
336 somewhat less Pb isotopic variability in Mangaia melt inclusions (Figure 3). Our suggestion is  
337 also in agreement with petrographic observations of resorption features on Ol and Px  
338 phenocrysts from M4, M10, M12, and M13 (Woodhead, 1996), which are consistent with  
339 magma mixing.

340

#### 341 4.3 Nature and age of the recycled components

342

343 The HIMU mantle reservoir is generally thought to reflect mantle mixed with subducted  
344 oceanic crust that experienced sulfide loss, causing depletion in Pb (Chauvel et al., 1992;  
345 Lassiter et al., 2003; Kelley et al., 2005); however, some proposals also call for a mantellic  
346 origin (Thirlwall, 1997), formation by recycled carbonate (Castillo, 2015; Castillo, 2016; Castillo  
347 et al., 2018), recycled serpentinites (Kendrick et al., 2017), carbonatitic metasomatism of the  
348 subcontinental lithospheric mantle that in turn delaminated and sank to the core-mantle boundary  
349 (Weiss et al., 2016), or an origin in metasomatic veins hosted in ancient subducted mantle  
350 lithosphere (Pilet et al., 2008). A wide range of ages have been proposed for the U/Pb  
351 fractionation that generated HIMU (~550 Ma to 3.0 Ga - (Hauri and Hart, 1993; Thirlwall, 1997;

352 Nebel et al., 2013; Mazza et al., 2019). Below, we offer a hypothetical scenario that allows the S-  
353 isotope data to be reconciled in light of the most common model for HIMU source generation:  
354 altered oceanic crust (AOC)+peridotite+a carbonated contribution (e.g. Jackson and Dasgupta,  
355 2008)

#### 356 *4.3.1 Subduction processes*

357 When including an AOC component, we must consider the potential effect of sulfide loss  
358 during slab subduction on  $\delta^{34}\text{S}$ . If a parcel of subducted oceanic crust started with  $\sim 1000$  ppm S  
359 (Rouxel et al., 2008a; Alt and Shanks, 2011) with an average  $\delta^{34}\text{S}$  of  $+3\text{‰}$  (Alt, 1995), and  
360 assuming Pb is hosted in sulfides (Kelley et al., 2003), Pb loss by sulfide breakdown in the  
361 subduction zone results in 400-20 ppm S (i.e. 60% to 98% sulfide loss) in the HIMU mantle  
362 source. A process resulting in the preferential loss of  $^{34}\text{S}$  could explain the unusually low  $\delta^{34}\text{S}$   
363 observed at Mangaia. Assuming 60% sulfide loss occurred during slab devolatilization, such  
364 would require an average fractionation of  $\sim 14\text{‰}$  between the fluid (preferentially partitioning  
365  $^{34}\text{S}$ ) and the residual slab (preferentially retaining  $^{32}\text{S}$ ) to explain our data, and a  $\sim 34\text{‰}$  fluid-  
366 slab residue fractionation<sup>1</sup> to explain the lowest  $\delta^{34}\text{S}$  in Cabral et al. (2013). If 98% of sulfide  
367 was lost, an average fractionation of  $\sim 9\text{‰}$  between the fluid and the residual slab to explain our  
368 data, and a  $\sim 21\text{‰}$  fluid-slab residue fractionation to explain the lowest  $\delta^{34}\text{S}$  in Cabral et al.  
369 (2013). These fractionations are large for temperatures associated with slab dehydration, and are  
370 not observed in studies of metamorphism (Li et al., 2020). We note additionally that in diamond  
371 sulfides, subducted components typically do not show evidence for S isotopic fractionation  
372 associated with subduction of MIF-Sulfur, displaying  $\delta^{34}\text{S} \geq 0$  and  $\Delta^{33}\text{S} \geq 0$  (Farquhar et al.,  
373 2002; Thomassot et al., 2009; Smit et al., 2019) and at localities where  $\delta^{34}\text{S}$  is fractionated

---

<sup>1</sup> This calculation represents an upper limit. Instrumental bias during analytical sessions results in a fractionation on  $\delta^{34}\text{S}$  as large as  $-3.8 \pm 0.7$  (1SD) (Cabral et al., 2013) when calibrating pyrrhotite measurements.

374 (Hofmann et al., 2009; Labidi et al., 2013; Labidi et al., 2015; Thomassot et al., 2015; Roerdink  
375 et al., 2016; Beaudry et al., 2018), the composition is attributed to that of the protolith and not  
376 subduction processes. In our study we adopt this interpretation and conclude that while sulfide  
377 breakdown in subduction zones causes U/Pb fractionation in HIMU, it may not account for  
378 variable  $\delta^{34}\text{S}$  observed globally, between Mangaia (this study; Cabral et al., 2013) and other  
379 HIMU locations (e.g. Beaudry et al. 2018).

#### 380 *4.3.2 Mixing AOC, peridotitic mantle, and a carbonated component*

381 The variable  $\delta^{34}\text{S}$  values of HIMU may be inherited from the composition of the  
382 protoliths, prior to subduction. Modern AOC has, on average, a  $\delta^{34}\text{S}$  that is positive due to the  
383 widespread occurrence of massive hydrothermal sulfides that generally carry positive values  
384 (Alt, 1995). While such material is consistent with the positive  $\delta^{34}\text{S}$  estimated for HIMU at other  
385 localities (e.g. (Labidi et al., 2014; Labidi and Cartigny, 2016), it contrasts with the low  $\delta^{34}\text{S}$   
386 values in HIMU Mangaia samples observed here. The bulk  $\delta^{34}\text{S}$  composition of the first  
387 kilometer of oceanic crust is estimated at -6 to -7 ‰ (Rouxel et al., 2008b; Alt and Shanks,  
388 2011), with positive  $\Delta^{33}\text{S}$  up to  $+0.162\text{‰} \pm 0.014$  (Ono et al., 2012). This first kilometer is where  
389 the deep biosphere is able to process seawater sulfate and precipitate biogenic sulfides. If this  
390 portion of the slab is the contributor of the AOC component in HIMU, such can explain the low  
391  $\delta^{34}\text{S}$  values at Mangaia with the caveat that a unique process is required to contribute a specific  
392 parcel of a slab (specially the upper portion) to the Mangaia mantle source.

393 An additional component we must consider in that of the carbonated component in  
394 HIMU lavas (Jackson and Dasgupta, 2008 and references therein). Cabral et al. (2014) argue for  
395 a carbonated source at HIMU Mangaia on the basis of inferred (pre-degassing) high primary  
396  $\text{CO}_2$  in melt inclusions that are required to explain their elevated  $\text{CaO}/\text{Al}_2\text{O}_3$  and low  $\text{SiO}_2$ , as

397 well as the presence of carbonatite observed in Mangaia melt inclusions by Saal et al. (1998) and  
398 Yurimoto et al., (2004). Castillo et al. (2018) suggest a component of recycled carbonate in the  
399 source of HIMU and such may be the source of carbonation for the HIMU mantle source. If the  
400 carbonated component originates from marine carbonates, or carbonated shales, as suggested by  
401 Castillo et al. (2018), they could have influenced the isotopic composition of sulfides. Archean  
402 and Proterozoic carbonates are not typically sulfide rich (Veizer et al., 1989; Veizer et al., 1992b;  
403 Veizer et al., 1992a) and frequently possess positive  $\delta^{34}\text{S}$ ; thus these lithologies do not provide an  
404 obvious way to connect the carbonated component to the full negative  $\delta^{34}\text{S}$  at Mangaia; however,  
405 the possibility of such a connection remains.

406 We can establish a simple mass balance of the carbonated component and AOC  
407 component in the HIMU mantle source. In our scenario, the carbonated component has a  $\delta^{34}\text{S}$  of  
408  $\approx -7.5\text{‰}$  (figure 1) and  $< 10,000$  ppm S estimated from carbonatite sulfur contents as a proxy for  
409 the carbonated component (Gold, 1963), the AOC component also has a  $\delta^{34}\text{S}$  of  $\approx -7.5\text{‰}$  (figure  
410 1) but  $< 400$  ppm S (Labidi et al., 2014), and the peridotitic mantle has a  $\delta^{34}\text{S}$  of  $= 0\text{‰}$  and 200  
411 ppm S (Lorand and Luguet, 2016). It is clear that regardless of the AOC-peridotite mixing ratio,  
412 the S isotope budget would be dominated by relatively small contributions of the carbonated  
413 component, irrespective of the  $\delta^{34}\text{S}$  compositions of AOC and peridotite. The AOC contribution  
414 was suggested to be as high as 50% in the source of Mangaia (Hauri and Hart, 1993). We suggest  
415 that in addition to 50% recycled AOC in the HIMU mantle source,  $< 10\%$  of the carbonated  
416 material is necessary to satisfy our mixing model (figure 1), in line with numerous suggestions  
417 for a C-rich component in the Mangaia mantle source (e.g., Saal et al., 1998; Yurimoto et al.,  
418 2004; Jackson and Dasgupta, 2008; Cabral et al., 2014).

419

420 *4.3.3 Unusual  $\delta^{34}\text{S}$  in HIMU OIB*

421 The contribution of negative  $\delta^{34}\text{S}$  components at Mangaia is unusual. It contrasts with  
422 recycled components observed at Samoa (EM II) and Discovery (EM I) hotspots, where positive  
423  $\delta^{34}\text{S}$  values are observed (Labidi et al., 2013; Labidi et al., 2015; Dottin III et al., 2020). Another  
424 HIMU hotspot, the Canary Islands, also shows a mantle source with positive  $\delta^{34}\text{S}$  values  
425 (Beaudry et al., 2018), and MORBs that incorporate variable amounts of HIMU components  
426 (Sobolev et al., 2007) appear to be influenced by a source with  $\delta^{34}\text{S} = +3 \pm 2\text{‰}$  (Labidi et al.,  
427 2014; Labidi and Cartigny, 2016). Importantly, the unusual  $^{34}\text{S}$ -depleted signature present in the  
428 Mangaia samples (this study and Cabral et al., 2013), as well as the EM1 Pitcairn lavas in  
429 Delavault et al. (2016), are associated with variable  $\Delta^{33}\text{S}$  that may be linked to the ages of the  
430 contributing source components.

431 It has been suggested that recycling of negative  $\delta^{34}\text{S}$  components may have occurred in  
432 the Archean (Cabral et al., 2013; Delavault et al., 2016; Farquhar and Jackson, 2016) and the  
433 Proterozoic (Canfield, 2004) as a way to offset the positive  $\delta^{34}\text{S}$  components observed in  
434 sediments. Negative  $\delta^{34}\text{S}$  values are not typically observed in Archean rocks, although they have  
435 been observed among positive  $\delta^{34}\text{S}$  values in some formations, such as barite deposits (Roerdink  
436 et al., 2016), gabbros (Thomassot et al., 2015), Archean conglomerates (Hofmann et al., 2009),  
437 and metamorphosed Archean crust (Kitayama et al., 2012). This hypothesis posits an under-  
438 represented reservoir of  $^{34}\text{S}$ -depleted material was lost to recycling and stored in the deep mantle,  
439 in the source of hotspots like Mangaia. EM-2 and EM-1 locations, where sedimentary recycling  
440 is suspected to occur, show the contribution of a crustal component with positive  $\delta^{34}\text{S}$  and near-  
441 zero  $\Delta^{33}\text{S}$  (Labidi et al., 2013; Labidi et al., 2015) and negative  $\delta^{34}\text{S}$  associated with variable  
442  $\Delta^{33}\text{S}$  (Delavault et al., 2016), respectively. Thus evidence from mantle samples suggests

443 recycling of sulfur with both negative and positive  $\delta^{34}\text{S}$ . Our measurements, along with those of  
444 Cabral et al. (2014), indicated that at Mangaia the negative  $\delta^{34}\text{S}$  dominates.

#### 445 *4.3.4 Information on relative age from $\Delta^{36}\text{S}$ data*

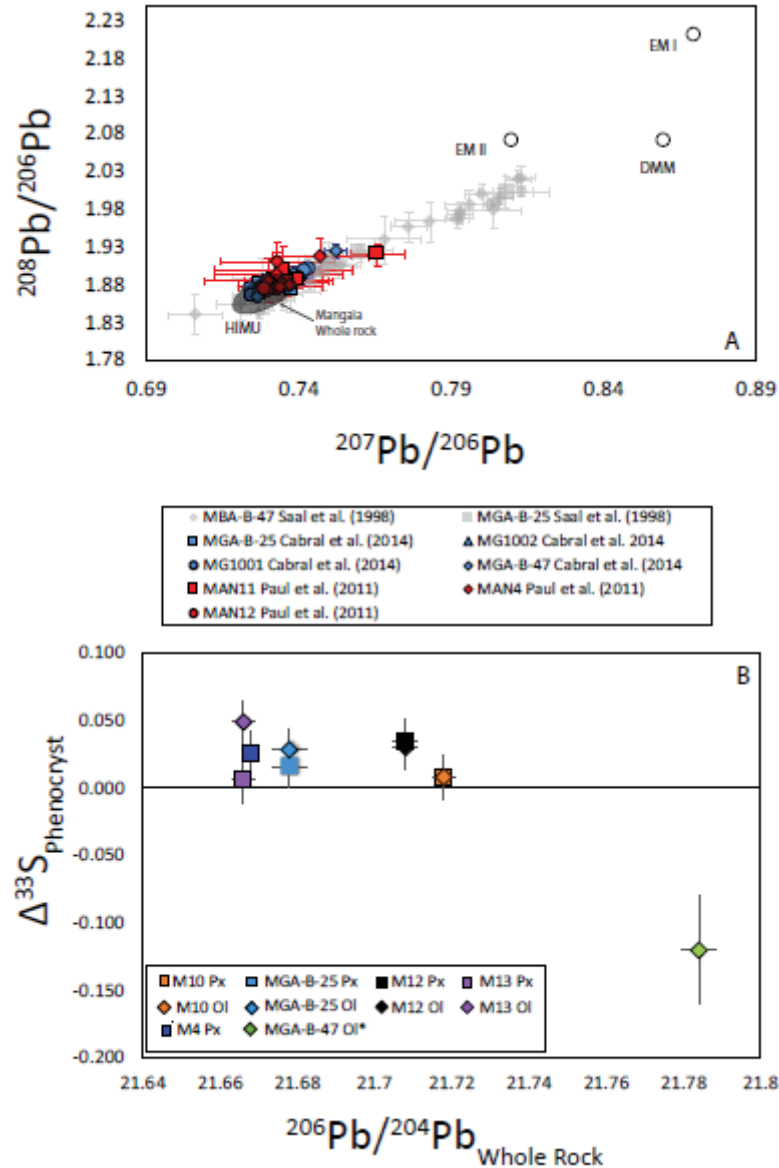
446 Additional constraints on the relative age of sulfur contributing slightly positive  $\Delta^{33}\text{S}$   
447 may be provided by the relationship between  $\Delta^{33}\text{S}$  and  $\Delta^{36}\text{S}$ . Archean rocks typically show  
448 covariation of  $\Delta^{33}\text{S}$  and  $\Delta^{36}\text{S}$  with a slope of  $\sim -1$  (Farquhar et al., 2007). This means that if a  
449  $\Delta^{33}\text{S}$  0.05‰, like that observed here, results from the contribution of an Archean protolith in the  
450 Mangaia mantle source, the corresponding  $\Delta^{36}\text{S}$  is predicted to be -0.05‰, which is not resolved  
451 with our uncertainty on  $\Delta^{36}\text{S}$  ( $\pm 0.3\%$ ). Post-Archean rocks show covariation of  $\Delta^{33}\text{S}$  and  $\Delta^{36}\text{S}$   
452 with a slope of  $\sim -7$ , which would result in a very small  $\Delta^{36}\text{S}$  shift to -0.4‰, which would be  
453 marginally resolvable given our estimated uncertainty. Our data generally plot below (more  
454 negative  $\Delta^{36}\text{S}$ ) and to the right (more positive  $\Delta^{33}\text{S}$ ) of typical MORB (Figure 2). The shift for  
455  $\Delta^{36}\text{S}$  of the data cluster is more consistent with a biological fractionation than a mass-  
456 independent (Archean) fractionation, but an Archean component with little to no mass-  
457 independent anomaly could satisfy our observations. However, we argue the most parsimonious  
458 explanation for the data here is that the material we measured is post-Archean, in addition to the  
459 contribution of Archean S (as identified in Cabral et al., 2013) in the MGA-B-25 data presented  
460 here. We note that the data do, however, have large uncertainties and our hypothesis would need  
461 to be confirmed with further analyses.

462

## 463 4.4 Recycling two reservoir ages

464

465 With the samples presented here, the Pb isotope data of whole rock basalts from  
466 Woodhead (1996) and Hauri and Hart (1993) all show extreme  $^{206}\text{Pb}/^{204}\text{Pb}$ , indicating the  
467 endmember HIMU character of the Mangaia mantle source, consistent with modern geochemical  
468 studies of Mangaia lavas (Hanyu et al., 2011 and references therein). Further constraints on the  
469 nature of the recycled components at Mangaia may be provided in relationships  
470 between  $^{206}\text{Pb}/^{204}\text{Pb}$  and sulfur isotopes: whole rock Pb isotope and bulk sulfide S isotope  
471 measurements reveal heterogeneity in Mangaia lavas. There is some Pb isotopic heterogeneity in  
472 the whole rocks, but the Pb isotope compositions of individual melt inclusions in Mangaia lavas  
473 reveal substantially more heterogeneity than the whole rock data (Saal et al., 1998; Yurimoto et  
474 al., 2004) though recent reports of Pb-isotopic heterogeneity in Mangaia inclusions reveal  
475 somewhat less heterogeneity (Paul et al., 2011; Cabral et al., 2014) (Figure 3a). Thus, compared  
476 to the bulk olivine and clinopyroxene analyses presented here, the greater S isotopic  
477 heterogeneity in individual melt inclusions (Cabral et al., 2013) may not be surprising in this  
478 light. Additionally, the remarkable  $\delta^{34}\text{S}$  disequilibrium between olivine and pyroxene in a single  
479 sample (this study) support a scenario in which the melt inclusions are sampling isotopically  
480 heterogenous compositions, as supported by the Pb-isotopic heterogeneity in Mangaia melt  
481 inclusions.



482

483

484 Figure 3. Whole rock Pb isotopes of Mangaia lavas, Pb isotopes in olivine-hosted melt inclusions  
 485 from Mangaia, and  $\Delta^{33}\text{S}$  of sulfide in melt inclusions within olivine and pyroxene phenocrysts.  
 486 A.)  $^{208}\text{Pb}/^{206}\text{Pb}$  versus  $^{207}\text{Pb}/^{206}\text{Pb}$  for olivine-hosted melt inclusions from Mangaia. Melt  
 487 inclusion data are published (Cabral et al., 2014; Paul et al., 2011; Saal et al., 1998), and whole  
 488 rock data are shown for reference (Hauri and Hart 1993; Woodhead, 1996). Data from melt  
 489 inclusions demonstrate Pb isotope heterogeneity in a single sample that suggests mixing of  
 490 multiple melt sources. B.)  $\Delta^{33}\text{S}$  versus  $^{206}\text{Pb}/^{204}\text{Pb}$ . Pb isotope data are from whole rock  
 491 measurements and S-isotope data represent bulk sulfide digestions of sulfur in melt inclusions  
 492 within olivine and pyroxene phenocrysts. \*The S measurement of bulk sulfide in olivine from  
 493 MGA-B-47 was presented in Cabral et al. (2013). The S isotope data and Pb isotope data show  
 494 potential for a relationship that suggest mixing of multiple S sources and would link MGA-B-47  
 495 to an older mantle component.

496  
497 Our S isotope data are from mineral separates extracted from the same whole rocks  
498 presented in Woodhead (1996) and Hauri and Hart (1993). Interestingly, the S isotope  
499 compositions presented in this study and Cabral et al., (2013) from mineral separates show the  
500 potential for a relationship between whole rock Pb isotopes and bulk S isotopes from mineral  
501 separates (figure 3b), where whole rock  $^{206}\text{Pb}/^{204}\text{Pb}$  increases with decreasing  $\Delta^{33}\text{S}$  in mineral  
502 separates. We note however that the whole rock Pb isotope data use an older TIMS method that  
503 did not employ double or triple spike to track in-run mass fractionation (Hauri and Hart, 1993;  
504 Woodhead, 1996). Thus, these older TIMS data are likely to have larger uncertainties than were  
505 originally reported by these authors (Hauri and Hart, 1993; Woodhead, 1996). Nonetheless, the  
506 variability in Pb isotope compositions of melt inclusions may be indicative of mixing of multiple  
507 compositions in the HIMU mantle source beneath Mangaia, suggesting the relationship we  
508 observe between bulk S isotope compositions from mineral separates and whole rock Pb isotope  
509 compositions, also reflects variability in the HIMU mantle source. If real, the data would reflect  
510 mixing between components of different ages, where higher  $^{206}\text{Pb}/^{204}\text{Pb}$  and the negative  $\Delta^{33}\text{S}$  in  
511 Mangaia is associated with an older mantle component.

512

## 513 **5 Conclusions**

514

515 The data presented here on sulfide inclusions within olivine and pyroxene phenocrysts  
516 from Mangaia reveal a heterogeneous S-isotope composition. Compositions range from -5.13‰  
517 to +0.21‰ ( $\pm 0.3$ ), +0.006‰ to +0.049‰ ( $\pm 0.016$ ), -0.81‰ to +0.69‰ ( $\pm 0.3$ ) for  $\delta^{34}\text{S}$ ,  $\Delta^{33}\text{S}$ , and  
518  $\Delta^{36}\text{S}$  respectively. The  $\Delta^{33}\text{S}$  values are different from those presented in Cabral et al. (2013) who  
519 generally show negative  $\Delta^{33}\text{S}$  and indicate that some, possibly the preponderance, of HIMU

520 sulfur sampled comes from a different reservoir, likely of younger post-Archean age. Both  
521 studies, however, report  $^{34}\text{S}$ -depleted sulfur, and this appears to be a characteristic of Mangaia  
522 HIMU that we attribute a crustal origin following observations by studies like Rouxel et al.  
523 (2008b) and Alt and Shanks (2011). Thus, there appears to be variability in the material derived  
524 from the same plume plumbing system at Mangaia.

525 This work focuses on S-isotope compositions of bulk sulfide in melt inclusions in Ol and  
526 Px from the same sample, and this sulfur is not in isotopic equilibrium but shows covariation in  
527  $\delta^{34}\text{S}$  and  $\Delta^{33}\text{S}$  which we link to the capturing of S-isotope compositions of various melts as they  
528 are added to the magma chamber. The data for Mangaia presented here, and provided by Cabral  
529 et al. (2013), support mixing of melts with at least 3 distinct sulfur isotope endmembers: 1.) A  
530 convective mantle component with  $\delta^{34}\text{S}=0$  and  $\Delta^{33}\text{S}=0$ ; 2.) a component with negative  $\delta^{34}\text{S}$  and  
531 slightly positive  $\Delta^{33}\text{S}$ ; and 3.) a component with negative  $\delta^{34}\text{S}$  and negative  $\Delta^{33}\text{S}$ .

### 532 **Acknowledgments**

533 We acknowledge funding for this project from NSF EAR-1348082 (to JF and MJ). Dataset for  
534 this manuscript exists as open access in the Digital Repository at the University of Maryland  
535 (DRUM) <https://doi.org/10.13016/zs1g-knnj>.  
536

### 537 **References**

- 538 Alt J. C. (1995) Sulfur isotopic profile through the oceanic crust: Sulfur mobility and seawater-  
539 crustal sulfur exchange during hydrothermal alteration. *Geology* **23**, 585–588.
- 540 Alt J. C. and Shanks W. C. (2011) Microbial sulfate reduction and the sulfur budget for a  
541 complete section of altered oceanic basalts, IODP Hole 1256D (eastern Pacific). *Earth*  
542 *Planet. Sci. Lett.* **310**, 73–83.
- 543 Antonelli M. A., Kim S.-T., Peters M., Labidi J., Cartigny P., Walker R. J., Lyons J. R., Hoek J.  
544 and Farquhar J. (2014) Early inner solar system origin for anomalous sulfur isotopes in  
545 differentiated protoplanets. *Proc. Natl. Acad. Sci. U. S. A.* **111**, 17749–54. Available at:  
546 <http://www.ncbi.nlm.nih.gov/pubmed/25453079>.
- 547 Beaudry P., Longpré M.-A., Economos R., Wing B. A., Bui T. H. and Stix J. (2018) Degassing-  
548 induced fractionation of multiple sulphur isotopes unveils post-Archaean recycled oceanic  
549 crust signal in hotspot lava. *Nat. Commun.* **9**, 5093.

- 550 Burgisser A., Alletti M. and Scaillet B. (2015) Simulating the behavior of volatiles belonging to  
551 the C–O–H–S system in silicate melts under magmatic conditions with the software D-  
552 Compress. *Comput. Geosci.* **79**, 1–14.
- 553 Cabral R. A., Jackson M. G., Koga K. T., Rose-Koga E. F., Hauri E. H., Whitehouse M. J., Price  
554 A. A., Day J. M. D., Shimizu N. and Kelley K. A. (2014) Volatile cycling of H<sub>2</sub>O, CO<sub>2</sub>, F,  
555 and Cl in the HIMU mantle: A new window provided by melt inclusions from oceanic hot  
556 spot lavas at Mangaia, Cook Islands. *Geochemistry, Geophys. Geosystems* **15**, 4445–4467.
- 557 Cabral R. A., Jackson M. G., Rose-Koga E. F., Koga K. T., Whitehouse M. J., Antonelli M. A.,  
558 Farquhar J., Day J. M. D. and Hauri E. H. (2013) Anomalous sulphur isotopes in plume  
559 lavas reveal deep mantle storage of Archaean crust. *Nature* **496**, 490–493.
- 560 Canfield D. E. (2004) The evolution of the Earth surface sulfur reservoir. *Am. J. Sci.* **304**, 839–  
561 861.
- 562 Cao X. and Liu Y. (2011) Equilibrium mass-dependent fractionation relationships for triple  
563 oxygen isotopes. *Geochim. Cosmochim. Acta* **75**, 7435–7445.
- 564 Castillo P. R. (2016) A proposed new approach and unified solution to old Pb paradoxes. *Lithos*  
565 **252**, 32–40.
- 566 Castillo P. R. (2015) The recycling of marine carbonates and sources of HIMU and FOZO ocean  
567 island basalts. *Lithos* **216**, 254–263.
- 568 Castillo P. R., MacIsaac C., Perry S. and Veizer J. (2018) Marine carbonates in the mantle source  
569 of Oceanic Basalts: Pb isotopic constraints. *Sci. Rep.* **8**, 1–7.
- 570 Chauvel C., Hofmann A. W. and Vidal P. (1992) HIMU-EM: the French Polynesian connection.  
571 *Earth Planet. Sci. Lett.* **110**, 99–119.
- 572 Craig J. R. and Kullerud G. (1968) Phase relations and mineral assemblages in the copper-lead-  
573 sulfur system. *Am. Mineral. J. Earth Planet. Mater.* **53**, 145–161.
- 574 Deines P. (2003) A note on intra-elemental isotope effects and the interpretation of non-mass-  
575 dependent isotope variations. *Chem. Geol.* **199**, 179–182.
- 576 Delavault H., Chauvel C., Thomassot E., Devey C. W. and Dazas B. (2016) Sulfur and lead  
577 isotopic evidence of relic Archean sediments in the Pitcairn mantle plume. *Proc. Natl.*  
578 *Acad. Sci.* **113**, 12952–12956.
- 579 Dottin III J. W., Labidi J., Lekic V., Jackson M. G. and Farquhar J. (2020) Sulfur isotope  
580 characterization of primordial and recycled sources feeding the Samoan mantle plume.  
581 *Earth Planet. Sci. Lett.* **534**, 116073.
- 582 Eldridge D. L. and Farquhar J. (2018) Rates and multiple sulfur isotope fractionations associated  
583 with the oxidation of sulfide by oxygen in aqueous solution. *Geochim. Cosmochim. Acta*  
584 **237**, 240–260.
- 585 Farquhar J. and Jackson M. (2016) Missing Archean sulfur returned from the mantle. *Proc. Natl.*  
586 *Acad. Sci.* **113**, 12893–12895.
- 587 Farquhar J., Wing B. A., McKeegan K. D., Harris J. W., Cartigny P. and Thiemens M. H. (2002)  
588 Mass-independent sulfur of inclusions in diamond and sulfur recycling on early Earth.  
589 *Science (5602)*. **298**, 2369–2372.

- 590 Fiege A., Holtz F., Behrens H., Mandeville C. W., Shimizu N., Crede L. S. and Göttlicher J.  
591 (2015) Experimental investigation of the S and S-isotope distribution between H<sub>2</sub>O–S±Cl  
592 fluids and basaltic melts during decompression. *Chem. Geol.* **393**, 36–54.
- 593 Gaetani G. A. and Grove T. L. (1997) Partitioning of moderately siderophile elements among  
594 olivine, silicate melt, and sulfide melt: constraints on core formation in the Earth and Mars.
- 595 Gaillard F., Scaillet B. and Arndt N. T. (2011) Atmospheric oxygenation caused by a change in  
596 volcanic degassing pressure. *Nature* **478**, 229–232.
- 597 Gold D. P. (1963) Average chemical composition of carbonatites. *Econ. Geol.* **58**, 988–991.
- 598 Hanyu T., Tatsumi Y., Senda R., Miyazaki T., Chang Q., Hirahara Y., Takahashi T., Kawabata  
599 H., Suzuki K. and Kimura J. (2011) Geochemical characteristics and origin of the HIMU  
600 reservoir: A possible mantle plume source in the lower mantle. *Geochemistry, Geophys.*  
601 *Geosystems* **12**.
- 602 Hauri E. H. and Hart S. R. (1993) ReOs isotope systematics of HIMU and EMII oceanic island  
603 basalts from the south Pacific Ocean. *Earth Planet. Sci. Lett.* **114**, 353–371.
- 604 Hofmann A., Bekker A., Rouxel O., Rumble D. and Master S. (2009) Multiple sulphur and iron  
605 isotope composition of detrital pyrite in Archaean sedimentary rocks: a new tool for  
606 provenance analysis. *Earth Planet. Sci. Lett.* **286**, 436–445.
- 607 Hulston J. R. and Thode H. G. (1965) Variations in the S S and S Contents of Meteorites and  
608 Their Relation to Chemical and Nuclear Effects. *Journal Geophys. Research* **70**, 3475–  
609 3484.
- 610 Jackson M. G. and Dasgupta R. (2008) Compositions of HIMU, EM1, and EM2 from global  
611 trends between radiogenic isotopes and major elements in ocean island basalts. *Earth*  
612 *Planet. Sci. Lett.* **276**, 175–186.
- 613 Jugo P. J., Wilke M. and Botcharnikov R. E. (2010) Sulfur K-edge XANES analysis of natural  
614 and synthetic basaltic glasses: Implications for S speciation and S content as function of  
615 oxygen fugacity. *Geochim. Cosmochim. Acta* **74**, 5926–5938.
- 616 Kelley K. A., Plank T., Farr L., Ludden J. and Staudigel H. (2005) Subduction cycling of U, Th,  
617 and Pb. *Earth Planet. Sci. Lett.* **234**, 369–383.
- 618 Kelley K. A., Plank T., Ludden J. and Staudigel H. (2003) Composition of altered oceanic crust  
619 at ODP Sites 801 and 1149. *Geochemistry, Geophys. Geosystems* **4**.
- 620 Kendrick M. A., Hémond C., Kamenetsky V. S., Danyushevsky L., Devey C. W., Rodemann T.,  
621 Jackson M. G. and Perfit M. R. (2017) Seawater cycled throughout Earth's mantle in  
622 partially serpentinized lithosphere. *Nat. Geosci.* **10**, 222–228.
- 623 Kitayama Y., Thomassot E., O'Neil J. and Wing B. A. (2012) Sulfur- and oxygen-isotope  
624 constraints on the sedimentary history of apparent conglomerates from the Nuvvuagittuq  
625 Greenstone Belt (Nunavik, Québec). *Earth Planet. Sci. Lett.* **355**, 271–282.
- 626 Labidi J. and Cartigny P. (2016) Negligible sulfur isotope fractionation during partial melting:  
627 Evidence from Garrett transform fault basalts, implications for the late-veener and the  
628 hadean matte. *Earth Planet. Sci. Lett.* **451**, 196–207.
- 629 Labidi J., Cartigny P., Birck J. L., Assayag N. and Bourrand J. J. (2012) Determination of

- 630 multiple sulfur isotopes in glasses: a reappraisal of the MORB  $\delta^{34}\text{S}$ . *Chem. Geol.* **334**,  
631 189–198.
- 632 Labidi J., Cartigny P., Hamelin C., Moreira M. and Dosso L. (2014) Sulfur isotope budget ( $^{32}\text{S}$ ,  
633  $^{33}\text{S}$ ,  $^{34}\text{S}$  and  $^{36}\text{S}$ ) in Pacific-Antarctic ridge basalts: A record of mantle source  
634 heterogeneity and hydrothermal sulfide assimilation. *Geochim. Cosmochim. Acta* **133**, 47–  
635 67. Available at: <http://dx.doi.org/10.1016/j.gca.2014.02.023>.
- 636 Labidi J., Cartigny P. and Jackson M. G. (2015) Multiple sulfur isotope composition of oxidized  
637 Samoan melts and the implications of a sulfur isotope ‘mantle array’ in chemical  
638 geodynamics. *Earth Planet. Sci. Lett.* **417**, 28–39.
- 639 Labidi J., Cartigny P. and Moreira M. (2013) Non-chondritic sulphur isotope composition of the  
640 terrestrial mantle. *Nature* **501**, 208–211. Available at:  
641 <http://dx.doi.org/10.1038/nature12490>.
- 642 Lassiter J. C., Blichert-Toft J., Hauri E. H. and Barszczus H. G. (2003) Isotope and trace element  
643 variations in lavas from Raivavae and Rapa, Cook–Austral islands: constraints on the nature  
644 of HIMU-and EM-mantle and the origin of mid-plate volcanism in French Polynesia. *Chem.*  
645 *Geol.* **202**, 115–138.
- 646 Li Y., Yu H., Gu X., Guo S. and Huang F. (2020) Silicon isotopic fractionation during  
647 metamorphic fluid activities: constraints from eclogites and ultrahigh-pressure veins in the  
648 Dabie orogen, China. *Chem. Geol.* **540**, 119550.
- 649 Lorand J.-P. and Luguet A. (2016) Chalcophile and siderophile elements in mantle rocks: Trace  
650 elements controlled by trace minerals. *Rev. Mineral. Geochemistry* **81**, 441–488.
- 651 Mandeville C. W., Webster J. D., Tappen C., Taylor B. E., Timbal A., Sasaki A., Hauri E. and  
652 Bacon C. R. (2009) Stable isotope and petrologic evidence for open-system degassing  
653 during the climactic and pre-climactic eruptions of Mt. Mazama, Crater Lake, Oregon.  
654 *Geochim. Cosmochim. Acta* **73**, 2978–3012.
- 655 Mazza S. E., Gazel E., Bizimis M., Moucha R., Béguelin P., Johnson E. A., McAleer R. J. and  
656 Sobolev A. V. (2019) Sampling the volatile-rich transition zone beneath Bermuda. *Nature*  
657 **569**, 398–403.
- 658 Nebel O., Arculus R. J., van Westrenen W., Woodhead J. D., Jenner F. E., Nebel-Jacobsen Y. J.,  
659 Wille M. and Eggins S. M. (2013) Coupled Hf–Nd–Pb isotope co-variations of HIMU  
660 oceanic island basalts from Mangaia, Cook-Austral islands, suggest an Archean source  
661 component in the mantle transition zone. *Geochim. Cosmochim. Acta* **112**, 87–101.
- 662 Ono S., Keller N. S., Rouxel O. and Alt J. C. (2012) Sulfur-33 constraints on the origin of  
663 secondary pyrite in altered oceanic basement. *Geochim. Cosmochim. Acta* **87**, 323–340.
- 664 Paul B., Woodhead J. D., Hergt J., Danyushevsky L., Kunihiro T. and Nakamura E. (2011) Melt  
665 inclusion Pb-isotope analysis by LA–MC–ICPMS: assessment of analytical performance  
666 and application to OIB genesis. *Chem. Geol.* **289**, 210–223.
- 667 Peach C. L., Mathez E. A. and Keays R. R. (1990) Sulfide melt-silicate melt distribution  
668 coefficients for noble metals and other chalcophile elements as deduced from MORB:  
669 Implications for partial melting. *Geochim. Cosmochim. Acta* **54**, 3379–3389.
- 670 Pilet S., Baker M. B. and Stolper E. M. (2008) Metasomatized lithosphere and the origin of

- 671 alkaline lavas. *Science* (5878). **320**, 916–919.
- 672 Roerdink D. L., Mason P. R. D., Whitehouse M. J. and Brouwer F. M. (2016) Reworking of  
673 atmospheric sulfur in a Paleoproterozoic hydrothermal system at Londozi, Barberton  
674 Greenstone Belt, Swaziland. *Precambrian Res.* **280**, 195–204.
- 675 Rouxel O., Ono S., Alt J., Rumble D. and Ludden J. (2008a) Sulfur isotope evidence for  
676 microbial sulfate reduction in altered oceanic basalts at ODP Site 801. *Earth Planet. Sci.*  
677 *Lett.* **268**, 110–123.
- 678 Rouxel O., Shanks III W. C., Bach W. and Edwards K. J. (2008b) Integrated Fe- and S-isotope  
679 study of seafloor hydrothermal vents at East Pacific Rise 9–10 N. *Chem. Geol.* **252**, 214–  
680 227.
- 681 Saal A. E., Hart S. R., Shimizu N., Hauri E. H. and Layne G. D. (1998) Pb isotopic variability in  
682 melt inclusions from oceanic island basalts, Polynesia. *Science* (5393). **282**, 1481–1484.
- 683 Salters V. J. M. and Stracke A. (2004) Composition of the depleted mantle. *Geochemistry,*  
684 *Geophys. Geosystems* **5**.
- 685 Smit K. V., Shirey S. B., Hauri E. H. and Stern R. A. (2019) Sulfur isotopes in diamonds reveal  
686 differences in continent construction. *Science* (6438). **364**, 383–385.
- 687 Sobolev A. V., Hofmann A. W., Kuzmin D. V., Yaxley G. M., Arndt N. T., Chung S.-L.,  
688 Danyushevsky L. V., Elliott T., Frey F. A. and Garcia M. O. (2007) The amount of recycled  
689 crust in sources of mantle-derived melts. *Science* (5823). **316**, 412–417.
- 690 Sobolev A. V. and Shimizu N. (1993) Ultra-depleted primary melt included in an olivine from the  
691 Mid-Atlantic Ridge. *Nature* **363**, 151–154.
- 692 Thirlwall M. F. (1997) Pb isotopic and elemental evidence for OIB derivation from young HIMU  
693 mantle. *Chem. Geol.* **139**, 51–74.
- 694 Thomassot E., Cartigny P., Harris J. W., Lorand J. P., Rollion-Bard C. and Chaussidon M.  
695 (2009) Metasomatic diamond growth: A multi-isotope study (<sup>13</sup>C, <sup>15</sup>N, <sup>33</sup>S, <sup>34</sup>S) of  
696 sulphide inclusions and their host diamonds from Jwaneng (Botswana). *Earth Planet. Sci.*  
697 *Lett.* **282**, 79–90.
- 698 Thomassot E., O’Neil J., Francis D., Cartigny P. and Wing B. A. (2015) Atmospheric record in  
699 the Hadean Eon from multiple sulfur isotope measurements in Nuvvuagittuq Greenstone  
700 Belt (Nunavik, Quebec). *Proc. Natl. Acad. Sci.* **112**, 707–712.
- 701 Veizer J., Clayton R. N. and Hinton R. W. (1992a) Geochemistry of Precambrian carbonates: IV.  
702 Early Paleoproterozoic (2.25±0.25 Ga) seawater. *Geochim. Cosmochim. Acta* **56**, 875–885.
- 703 Veizer J., Hoefs J., Lowe D. R. and Thurston P. C. (1989) Geochemistry of Precambrian  
704 carbonates: II. Archean greenstone belts and Archean sea water. *Geochim. Cosmochim.*  
705 *Acta* **53**, 859–871.
- 706 Veizer J., Plumb K. A., Clayton R. N., Hinton R. W. and Grotzinger J. P. (1992b) Geochemistry  
707 of Precambrian carbonates: V. late Paleoproterozoic seawater. *Geochim. Cosmochim. Acta*  
708 **56**, 2487–2501.
- 709 Weiss Y., Class C., Goldstein S. L. and Hanyu T. (2016) Key new pieces of the HIMU puzzle  
710 from olivines and diamond inclusions. *Nature* **537**, 666–670.

- 711 Woodhead J. D. (1996) Extreme HIMU in an oceanic setting: The geochemistry of Mangaia  
712 Island (Polynesia), and temporal evolution of the Cook—Austral hotspot. *J. Volcanol.*  
713 *Geotherm. Res.* **72**, 1–19.
- 714 Workman R. K. and Hart S. R. (2005) Major and trace element composition of the depleted  
715 MORB mantle (DMM). *Earth Planet. Sci. Lett.* **231**, 53–72.
- 716 Yurimoto H., Kogiso T., Abe K., Barszczus H. G., Utsunomiya A. and Maruyama S. (2004) Lead  
717 isotopic compositions in olivine-hosted melt inclusions from HIMU basalts and possible  
718 link to sulfide components. *Phys. Earth Planet. Inter.* **146**, 231–242.
- 719
- 720
- 721
- 722

Figure 1.

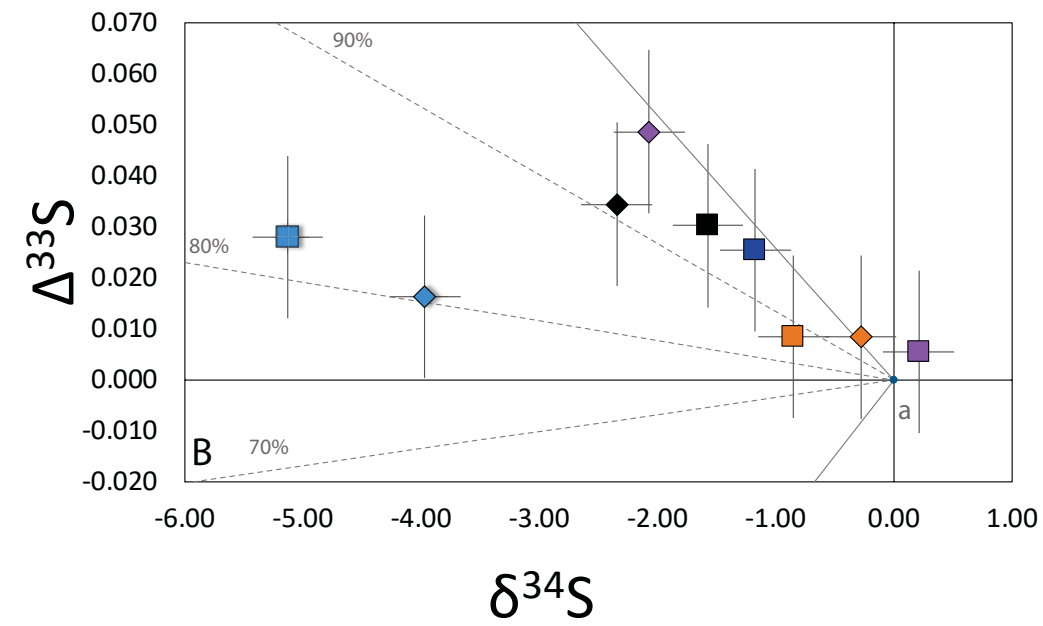
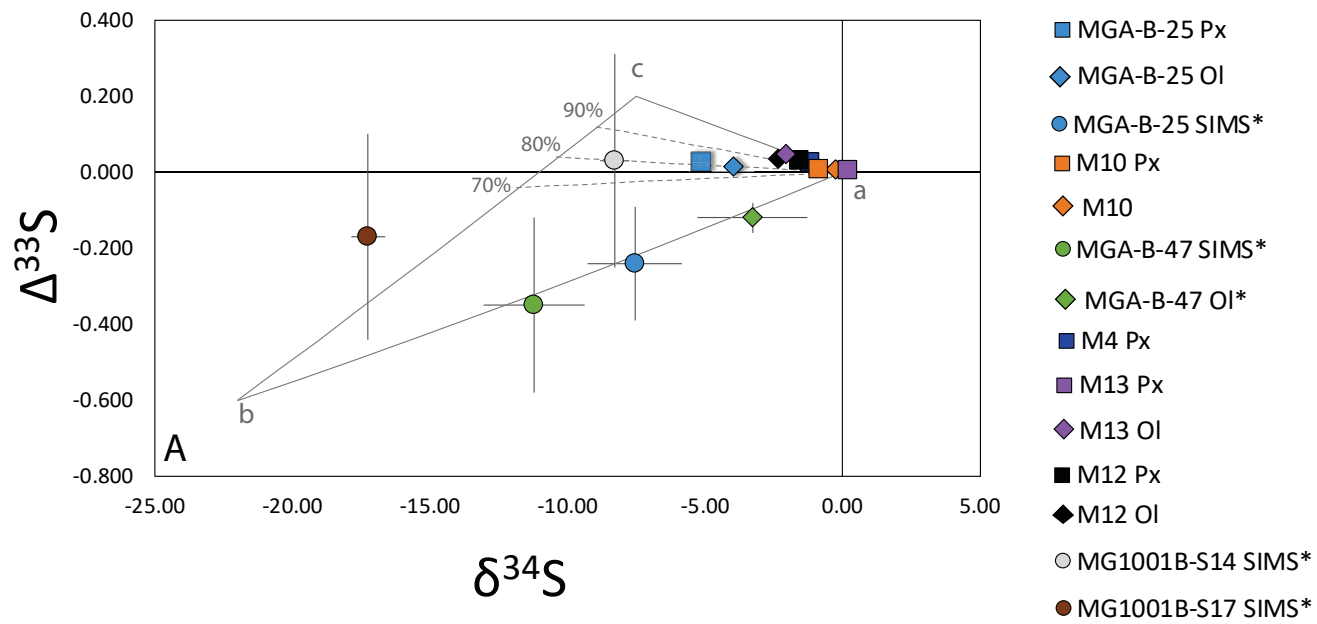


Figure 2.

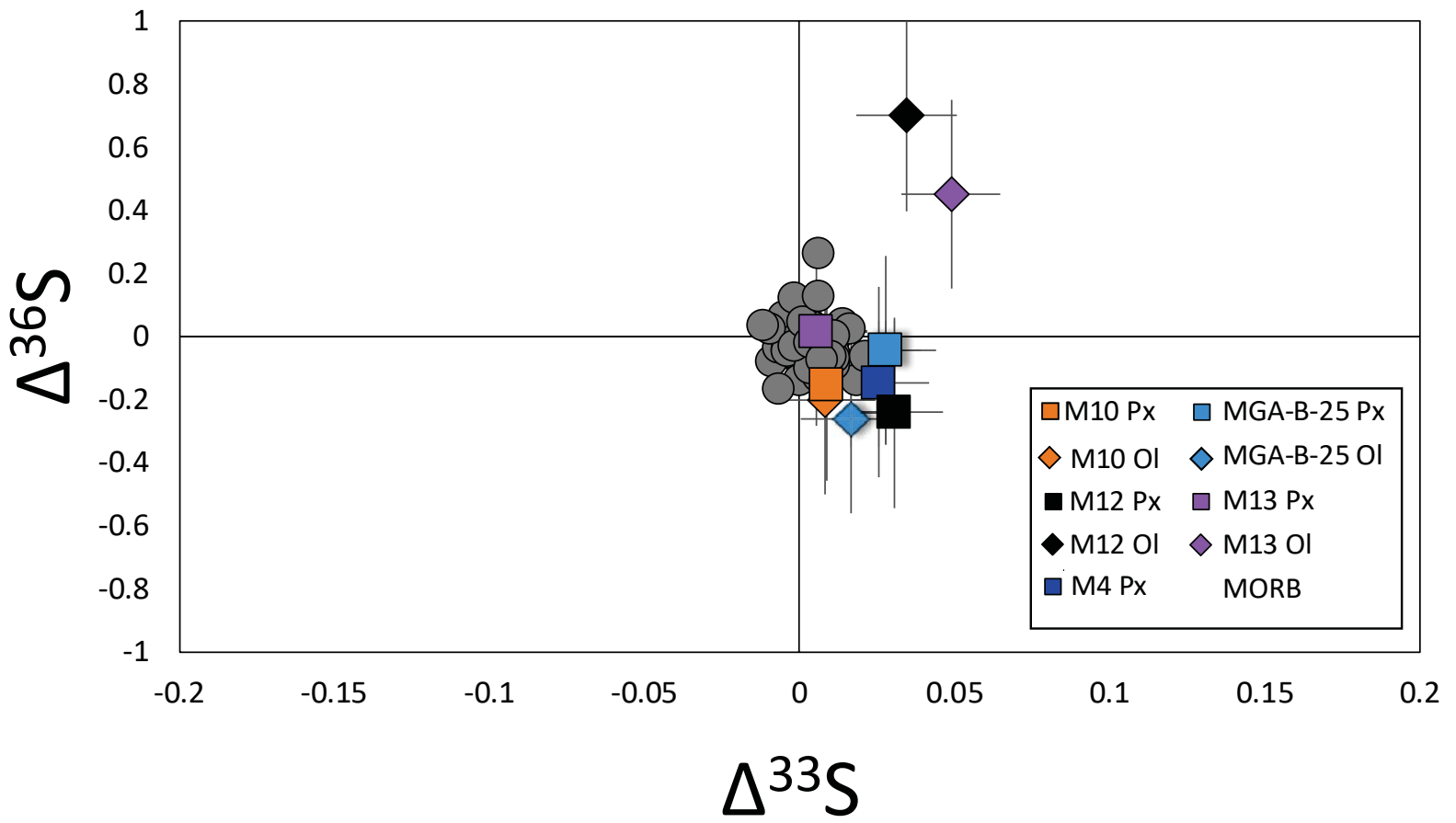
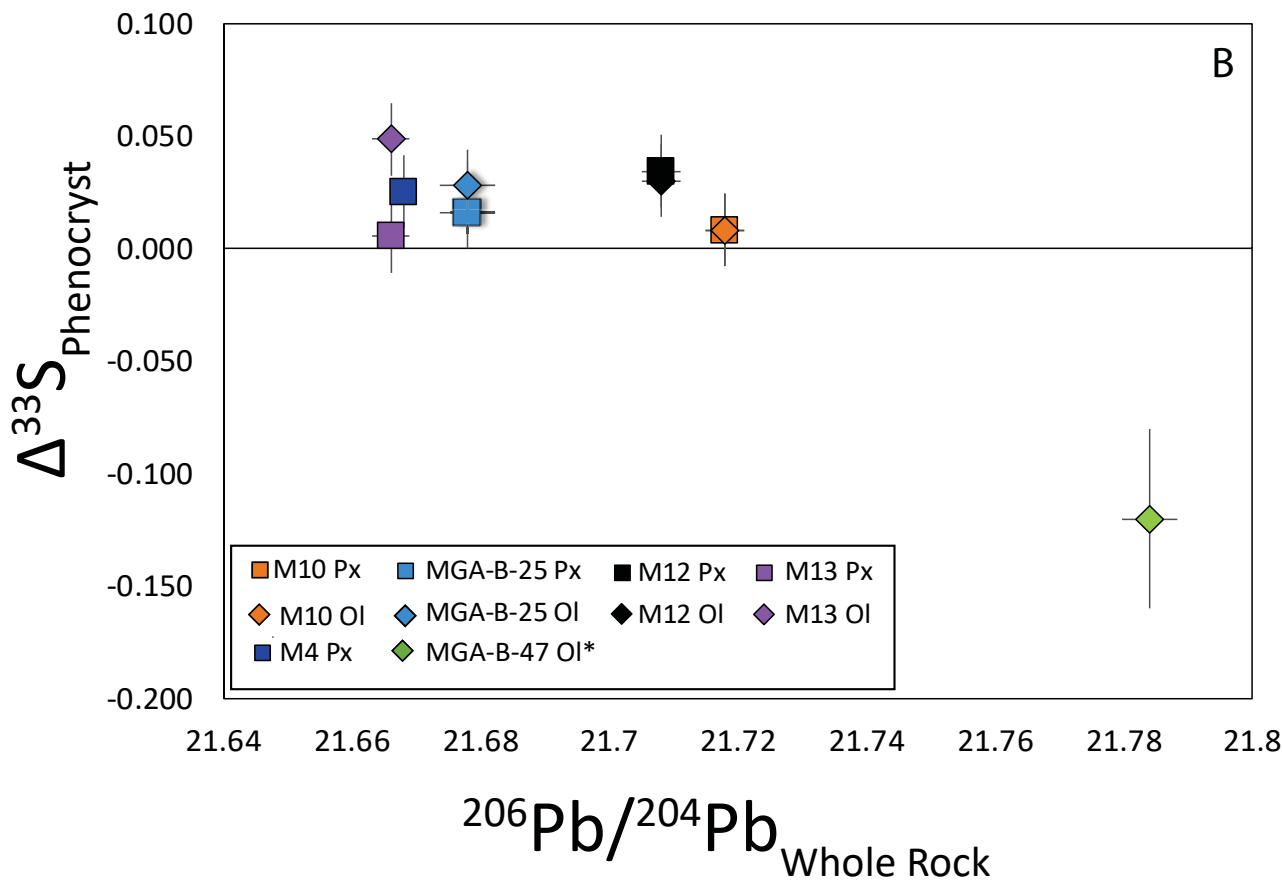
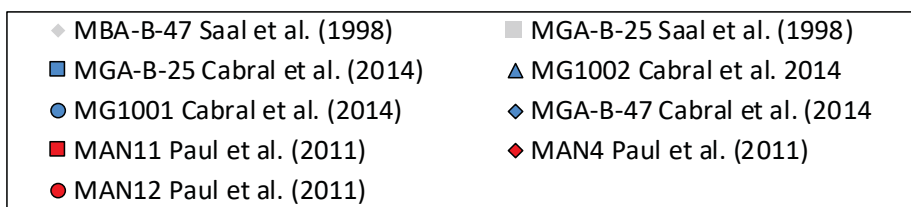
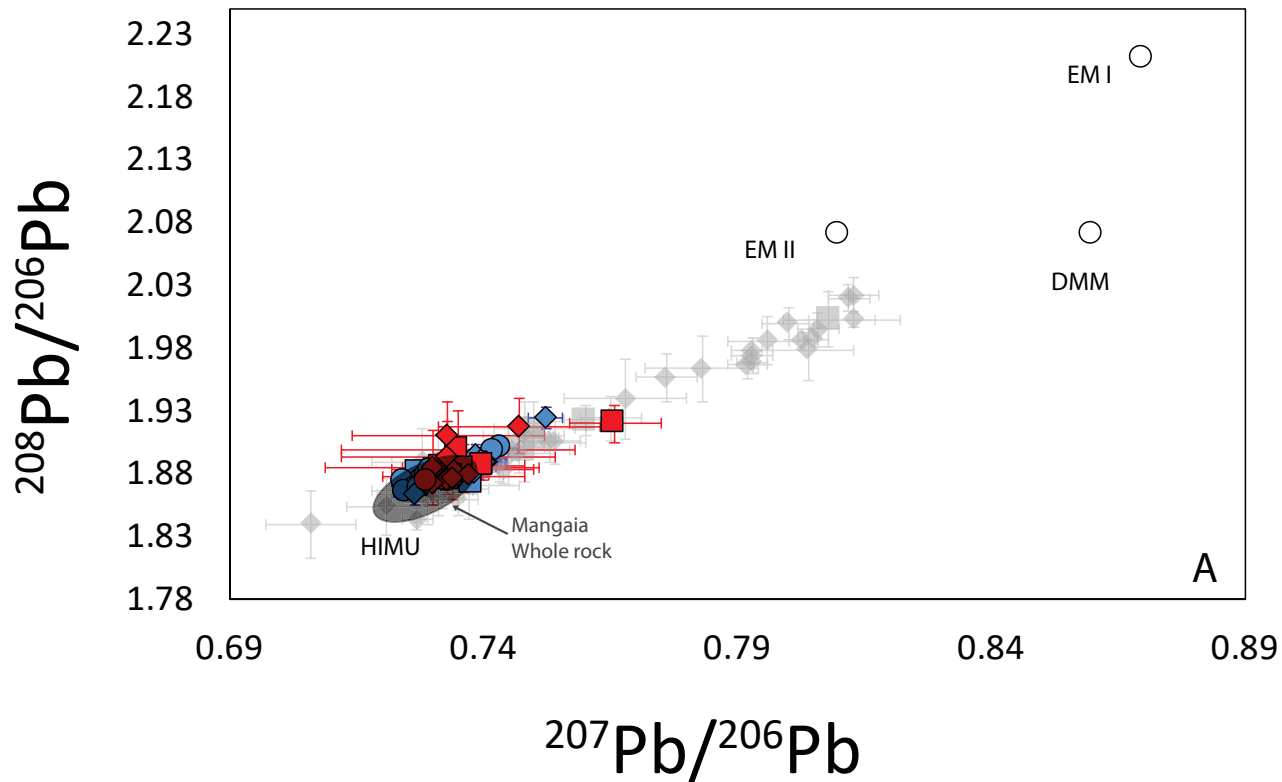


Figure 3.



**Table 1.** S-isotope compositions of bulk sulfide in Ol and Px separates f

Sample	Rock type	S (ppm)	$\delta^{34}\text{S}$	$\Delta^{33}\text{S}$	$\Delta^{36}\text{S}$
MGA-B-25 Px	Ankaramite	290	-5.1	0.028	0.0
MGA-B-25 Ol	Ankaramite	333	-4.0	0.016	-0.3
M4 Px	Ankaramite	185	-1.2	0.026	-0.1
M10 PX	Ankaramite	112	-0.8	0.009	-0.2
M10 OL	Ankaramite	161	-0.3	0.008	-0.2
M12 PX	Ankaramite	127	-1.6	0.030	-0.2
M12 OL	Ankaramite	322	-2.3	0.035	0.7
M13 PX	Ankaramite	238	0.2	0.006	0.0
M13 OL	Ankaramite	96	-2.1	0.049	0.5
MGA-B-47*	Picrite		-3.28	-0.13	

Table 1. Data compilation of S-isotope and radiogenic Pb isotope comp  
Radiogenic Pb for M4 -M13 from Woodhead et al. (1996). Radiogenic Pl  
Estimated coordinates are sourced from the GeoRoc database. Rock chi  
al. (1998).

from Mangaia Basalts

$^{206}\text{Pb}/^{204}\text{Pb}$	$^{207}\text{Pb}/^{204}\text{Pb}$	$^{208}\text{Pb}/^{204}\text{Pb}$	Latitude	Longitude
21.678	15.807	40.512	-21.9133	-157.914
21.678	15.807	40.512	-21.9133	-157.914
21.668	15.828	40.565	-21.93	-157.93
21.718	15.837	40.583	-21.93	-157.93
21.718	15.837	40.583	-21.93	-157.93
21.708	15.831	40.561	-21.93	-157.93
21.708	15.831	40.561	-21.93	-157.93
21.666	15.817	40.539	-21.93	-157.93
21.666	15.817	40.539	-21.93	-157.93
21.784	15.813	40.734	-21.9379	-157.923

positions presented. \*S-isotope data from Cabral et al. (2013).

b data for MGA-B-25 and MGA-B-47 from Hauri and Hart (1993).

aracterization sourced from Woodhead et al. (1996) and Saal et